

MONOSACCHARIDE DERIVATIVES:
SYNTHESIS, ANTIMICROBIAL, PASS, ANTIVIRAL AND MOLECULAR
DOCKING STUDIES AGAINST SARS-COV-2 M^{PRO} INHIBITORS

FARHANA YASMIN,* MOHAMMED R. AMIN,* MOHAMMED A. HOSEN,*
MOHAMMED Z. H. BULBUL,* SUJAN DEY** and SARKAR M. A. KAWSAR*

*Department of Chemistry, Faculty of Science, University of Chittagong,
Chittagong-4331, Bangladesh

**Department of Microbiology, Faculty of Biological Science, University of Chittagong,
Chittagong-4331, Bangladesh

✉ Corresponding author: S. M. A. Kawsar, akawsar@cu.ac.bd

Received April 15, 2021

Several carbohydrate-based drugs are currently being used to treat a number of diseases in humans worldwide. Thus, our research group has focused on the synthesis of new methyl α -D-mannopyranoside (MDM) derivatives and their antimicrobial evaluation through computational studies. A series of MDM derivatives (**2-6**) were synthesized through facile regioselective acylation, using the direct method affording 6-*O*-(3-chlorobenzoyl) derivatives. This isolated 6-*O*-derivative was further transformed to 2,3,4-tri-*O*-acyl derivatives, bearing a wide variety of functionalities in a single molecular framework. The structures of the newly designed molecules were elucidated with the aid of IR, ¹H NMR, mass spectroscopy, and elemental analysis. The prediction of the activity spectra for the compounds (PASS) and their *in vitro* antimicrobial evaluation were performed, demonstrating them to be potential antimicrobial agents. The antimicrobial tests demonstrated that the compounds **3** and **5** were the most potent with the minimum inhibitory concentration (MIC) values, ranging from 0.312±0.01 to 1.25±0.03 mg/mL, and minimum bactericidal concentration (MBC) values, ranging from 0.625±0.02 to 2.50±0.05 mg/mL. A quantum chemical study was performed to calculate the thermodynamic, molecular orbital and electrostatic potential properties of the designed compounds. Molecular docking simulation was carried out against SARS-CoV-2 M^{PRO} protein 7BQY and 6Y84 to investigate their binding energy and binding tactics with the viral protein, and better binding affinity than that of the parent drug was observed. Also, pharmacokinetic prediction revealed an improved drug-likeness profile for all MDM derivatives.

Keywords: mannopyranoside, synthesis, antimicrobial, PASS, molecular docking

INTRODUCTION

Scientists around the world are looking for more effective and safe antimicrobial agents for the cure of diseases caused by pathogenic organisms. For this reason, the synthesis of new chemicals and the investigation of their antimicrobial activity represent the best way to develop efficient antimicrobial agents. Besides synthesis, an *in vitro* comparative study of antibacterial activities was also carried out in this research.

Carbohydrates are key molecules in nature, with several roles in biological processes. For a long time, carbohydrates have been a very attractive topic for scientists due to their immense importance in biological systems, including viral

and bacterial infections, cell growth and proliferation, cell-cell communication, as well as immune response.^{1,2} They are the source of a metabolic energy supply, but also for the fine-tuning of cell-cell interactions and other crucial processes.^{3,4} It has been found from the literature survey that a large number of biologically active compounds also possess aromatic, heteroaromatic, and acyl substituents.⁵ The benzene, substituted benzene, and also nitrogen, sulfur, and halogen-containing substituents are known to enhance the biological activity of the parent compound.⁶ It is also known that, if an active nucleus is linked to another active nucleus, the resulting molecule may possess greater

potential for biological activity.⁵ Moreover, selective acylation of carbohydrates^{7,8} and the evaluation of microbial activities^{9,10} reveal that, in many cases, the combination of two or more heteroaromatic nuclei and acyl groups enhances the biological activity manifold, compared to that of the parent nucleus.^{11,12} In a recent study, some monosaccharide derivatives have been found to be potential inhibitors of cancer cell protein 4ZZZ.¹³

The recent outbreak of a novel coronavirus disease (COVID-19), occurring from a severe acute respiratory syndrome (SARS) caused by a coronavirus, started in Wuhan, China, is spreading rapidly in humans and has turned into a global pandemic.¹⁴ Modifications of the hydroxyl (-OH) group of the nucleoside structure revealed some potent SARS-CoV-2 candidates^{15,16} and antimicrobial agents.^{17,18} In this research, we have modified the hydroxyl (-OH) group of methyl α -D-mannopyranoside by some acyl substituents (aliphatic and aromatic), these modified derivatives have been optimized and their thermal, electrical stability and biochemical behavior have been assessed based on quantum mechanical methods. The free energy, enthalpy, entropy, heat capacity dipole-moment, HOMO-LUMO gap, DOS plot, polarizability, molar refractivity, atomic partial charge, and molecular electrostatic potential have been calculated to compare their thermal and chemical characteristics. The antimicrobial screening was performed for all compounds, with the prediction of PASS properties. Further, some selected derivatives (having better antibacterial and antifungal activity) were employed for molecular docking against SARS-CoV-2 main protease protein (PDB: 7BQY and 6Y84) to understand their nonbonding interactions, binding mode, and binding affinity. Finally, pharmacokinetic enumeration has been performed to compare their absorption, metabolism, and toxicity. The prime intention of our investigation was to understand the thermodynamic, molecular orbital, antimicrobial, binding mode, molecular electrostatic potential, physicochemical, and ADMET properties of MDM and its derivatives.

EXPERIMENTAL

Materials

Thin-layer chromatography (TLC) was performed on Kieselgel GF₂₅₄ (Germany), and the chromatogram was visualized by spraying the plates with 1% H₂SO₄, followed by heating the plates at 150-200 °C until

coloration appeared. Melting points (mp) were determined on an electrothermal melting point apparatus. FTIR spectral analyses were recorded using a Fourier-transform infrared spectrophotometer (Shimadzu, Japan) at the Department of Chemistry, University of Chittagong. Mass spectra of the synthesized compounds were obtained by liquid chromatography-electrospray ionization tandem mass spectrometry in positive ionization mode. A Bruker Advance DPX 400 MHz, using tetramethylsilane as an internal standard, was employed for recording the ¹H NMR spectra in CDCl₃ at WMSRC, JU, Bangladesh. Column chromatography was performed using silica gel G₆₀. CHCl₃/CH₃OH in different proportions was employed as solvent system for TLC analyses. All reagents used were commercially available from Sigma-Aldrich (Germany) and were used as received, unless otherwise specified. The following software was used in the present study: i) GaussSum 09, ii) GaussSum 3.0, iii) AutoDock 4.2.6, iv) Swiss-Pdb 4.1.0, v) Python 3.8.2, vi) Discovery Studio 3.5, vii) PyMOL 2.3, viii) ChemDraw Pro 12.0 (used to draw the two-dimensional structure of uridine derivatives), ix) pkCSM and PASS server (<http://biosig.unimelb.edu.au/pkcsm/static/img/pkcsm.png>), (<http://www.pharmaexpert.ru/passonline/>) and SwissADME free web tools (<http://www.swissadme.ch>) – employed to calculate the pharmacokinetic properties.

Synthesis of methyl 6-O-(3-chlorobenzoyl)- α -D-mannopyranoside (2)

A solution of the methyl α -D-mannopyranoside (1) (100 mg, 0.51 mmol) in anhydrous *N,N*-dimethylaniline (~3 mL) was cooled to 0 °C and treated with 1.1 molar equivalent of 3-chlorobenzoyl chloride (0.07 mL) and 4-Dimethylaminopyridine (DMAP) with continuous stirring by maintaining 0 °C temperature for 6 hours. Stirring was continued at room temperature. A few pieces of ice were added to the flask to destroy the excess reagent and then the contents were extracted with chloroform (3×10 mL). The combined CHCl₃ layer was washed successively with dilute HCl (10%), sat. aq. NaHCO₃ solution and distilled water. The organic layer was dried (MgSO₄), filtered and the filtrate was concentrated under reduced pressure. The resulting syrupy mass was subjected to silica gel column chromatographic purification (with CH₃OH/CHCl₃ = 1/8, v/v as eluent; *R_f* = 0.52) to provide the title compound (2) (170 mg, 88%) as needles, m.p. 110 °C.

Methyl 6-O-(3-chlorobenzoyl)- α -D-mannopyranoside (2)

IR (KBr) ν /cm⁻¹ 1689 (C=O), 3401-3469 (br) (-OH); ¹H NMR (400 MHz, CDCl₃) δ 8.00 (1H, d, *J* 7.5 Hz, Ar-H), 7.83 (1H, s, Ar-H), 7.46 (1H, d, *J* 7.7 Hz, Ar-H), 7.28 (1H, t, *J* 7.6 Hz, Ar-H), 5.48 (1H, m, H-6a), 4.83 (1H, m, H-6b), 4.69 (1H, s, H-1), 4.18 (1H, d,

J 3.2 Hz, H-2), 4.13 (1H, dd, *J* 3.1 and 9.3 Hz, H-3), 4.00 (1H, t, *J* 9.1 Hz, H-4), 3.59 (1H, m, H-5), 3.34 (3H, s, 1-OCH₃); LC-MS [M+1]⁺ 339.50; Analysis calcd. for C₁₄H₂₃O₇Cl: C, 49.65, H, 6.83%, found: C, 49.68, H, 6.81%.

General procedure for the synthesis of 2,3,4-tri-*O*-acyl derivatives (3-6)

To a cooled (-5 °C) and stirred solution of triol **2** (160 mg, 0.06 mmol) in dry *N,N*-dimethylaniline (3 mL) and DMAP, octanoyl chloride (0.05 mL, 3.5 molar eq.) was added and stirring was continued at this temperature for 5 hours. The reaction mixture was stirred with the addition of a few pieces of ice and extracted with chloroform. The organic layer was washed with 5% hydrochloric acid, saturated aqueous sodium hydrogen carbonate solution, and distilled water. The chloroform layer was dried with magnesium sulfate, filtered, and filtrate concentrated to leave a syrupy residue. The syrup was passed through a silica gel column and eluted with methanol-chloroform (1:8) to furnish the compound (**3**) (100 mg, 85%) as a pasty mass. A similar reaction of compounds **4**, **5**, and **6** afforded the lauroyl derivatives (120 mg, 85%) as a solid mass; palmitoyl derivative (120 mg, 85%) as a thick mass; trityl derivative (150 mg, 74%) as crystalline solid, m.p. (140-142 °C), respectively.

Methyl 6-*O*-(3-chlorobenzoyl)-2,3,4-tri-*O*-octanoyl- α -*D*-mannopyranoside (**3**)

IR (KBr) ν /cm⁻¹ 1688 (C=O); ¹H-NMR (400 MHz, CDCl₃) δ 7.60 (1H, d, *J* 7.6 Hz, Ar-H), 7.51 (1H, s, Ar-H), 7.41 (1H, d, *J* 7.6 Hz, Ar-H), 7.29 (1H, t, *J* 7.5 Hz, Ar-H), 5.05 (1H, s, H-1), 4.89 (1H, d, *J* 3.4 Hz, H-2), 4.78 (1H, dd, *J* 3.2 and 9.0 Hz, H-3), 4.61 (1H, t, *J* 9.0 Hz, H-4), 3.88 (1H, m, H-6a), 3.79 (1H, m, H-6b), 3.75 (1H, m, H-5), 3.45 (3H, s, 1-OCH₃), 2.40 {6H, m, 3×CH₃(CH₂)₅CH₂CO-}, 1.70 {6H, m, 3×CH₃(CH₂)₄CH₂CH₂CO-}, 1.30 {24H, m, 3×CH₃(CH₂)₄(CH₂)₂CO-}, 0.91 {9H, m, 3×CH₃(CH₂)₆CO-}; LC-MS [M+1]⁺ 717.50; Analysis calcd. for C₃₈H₆₅O₁₀Cl: C, 63.66, H, 9.07%, found: C, 63.68, H, 9.09%.

Methyl 6-*O*-(3-chlorobenzoyl)-2,3,4-tri-*O*-lauroyl- α -*D*-mannopyranoside (**4**)

IR (KBr) ν /cm⁻¹ 1686 (C=O); ¹H NMR (400 MHz, CDCl₃) δ 7.58 (1H, d, *J* 7.5 Hz, Ar-H), 7.32 (1H, s, Ar-H), 7.29 (1H, d, *J* 7.4 Hz, Ar-H), 7.10 (1H, t, *J* 7.4 Hz, Ar-H), 5.21 (1H, s, H-1), 4.96 (1H, d, *J* 3.5 Hz, H-2), 4.80 (1H, dd, *J* 3.2 and 9.0 Hz, H-3), 4.78 (1H, t, *J* 9.1 Hz, H-4), 3.92 (1H, m, H-6a), 3.76 (1H, m, H-6b), 3.65 (1H, m, H-5), 3.46 (3H, s, 1-OCH₃), 2.34 {6H, m, 3×CH₃(CH₂)₉CH₂CO-}, 1.70 {6H, m, 3×CH₃(CH₂)₈CH₂CH₂CO-}, 1.28 {48H, m, 3×CH₃(CH₂)₈CH₂CH₂CO-}, 0.90 {9H, m, 3×CH₃(CH₂)₁₀CO-}. LC-MS [M+1]⁺ 885.50; Analysis

calcd. for C₅₀H₈₉O₁₀Cl: C, 67.83, H, 10.07%, found: C, 67.86, H, 10.06%.

Methyl 6-*O*-(3-chlorobenzoyl)-2,3,4-tri-*O*-palmitoyl- α -*D*-mannopyranoside (**5**)

IR (KBr) ν /cm⁻¹ 1685 (C=O); ¹H-NMR (400 MHz, CDCl₃) δ 7.57 (1H, d, *J* 7.5 Hz, Ar-H), 7.52 (1H, s, Ar-H), 7.50 (1H, d, *J* 7.4 Hz, Ar-H), 7.48 (1H, t, *J* 7.4 Hz, Ar-H), 5.26 (1H, s, H-1), 4.93 (1H, d, *J* 3.6 Hz, H-2), 4.82 (1H, dd, *J* 3.4 and 9.1 Hz, H-3), 4.69 (1H, t, *J* 9.2 Hz, H-4), 3.97 (1H, m, H-6a), 3.78 (1H, m, H-6b), 3.68 (1H, m, H-5), 3.42 (3H, s, 1-OCH₃), 2.34 {6H, m, 3×CH₃(CH₂)₁₃CH₂CO-}, 1.25 {78H, m, 3×CH₃(CH₂)₁₃CH₂CO-}, 0.90 {9H, m, 3×CH₃(CH₂)₁₄CO-}; LC-MS [M+1]⁺ 1053.50; Analysis calcd. for C₆₂H₁₁₃O₁₀Cl: C, 70.69, H, 10.74%, found: C, 70.71, H, 10.77%.

Methyl 6-*O*-(3-chlorobenzoyl)-2,3,4-tri-*O*-trityl- α -*D*-mannopyranoside (**6**)

IR (KBr) ν /cm⁻¹ 1681 (C=O); ¹H-NMR (400 MHz, CDCl₃) δ 7.68 (1H, d, *J* 7.4 Hz, Ar-H), 7.54 (18H, m, 3×Ar-H), 7.51 (1H, s, Ar-H), 7.47 (1H, d, *J* 7.4 Hz, Ar-H), 7.45 (1H, t, *J* 7.5 Hz, Ar-H), 7.35 (27H, m, 3×Ar-H), 5.22 (1H, s, H-1), 4.95 (1H, d, *J* 3.5 Hz, H-2), 4.85 (1H, dd, *J* 3.5 and 9.1 Hz, H-3), 4.65 (1H, t, *J* 9.2 Hz, H-4), 3.95 (1H, m, H-6a), 3.76 (1H, m, H-6b), 3.66 (1H, m, H-5), 3.41 (3H, s, 1-OCH₃); LC-MS [M+1]⁺ 1065.50; Analysis calcd. for C₇₁H₆₅O₇Cl: C, 80.04, H, 6.11%, found: C, 80.05, H, 6.13%.

Antimicrobial activities

Some partially protected derivatives of MDM (Scheme 1) were selected and screened for the antimicrobial activities against human pathogenic bacteria and plant pathogenic fungi. The bacterial and fungal pathogens, which were exposed to the chemicals under investigation, were collected from the Department of Microbiology, University of Chittagong.

Antibacterial susceptibility

The disc diffusion method¹⁹ was employed *in vitro* for determining the antibacterial susceptibility of the newly synthesized MDM derivatives (Scheme 1). In the disc diffusion method, paper discs of 4 mm in diameter and glass Petri plates of 90 mm in diameter were used during the whole experiment. The synthesized compounds and standard antibiotics were dissolved in sterile 5% (w/v) dimethyl sulfoxide (DMSO) for the preparation of the desired concentrated solution. After soaking the paper discs with the test chemicals in a solution of 24 mg/mL concentration, the discs were placed on swabbed Mueller-Hinton agar media (MHA). The plates were then incubated at 37 °C to allow the growth of the test organisms and observed after 24 h. Each experiment was performed in triplicate. In this experiment, a positive control was maintained with azithromycin

(BEXIMCO, Bangladesh Ltd.) and a negative control was maintained with DMSO.

Determination of MIC and MBC

The minimum inhibitory concentration (MIC) was determined as per the guidelines adopted by the Clinical and Laboratory Standards Institute (CLSI).²⁰ For this purpose, the twofold serial dilution technique was followed. The microbial growth in the well was detected by an indicator of 10 μ L of 2, 3, 5-triphenyltetrazolium chloride (TTC) with 0.5% (w/v) solution. The MIC was confirmed as the concentration of the last well where there was no microbial growth. From this experiment, the content of the wells was sown on plates with Mueller-Hinton agar medium to establish the minimum bactericidal concentration (MBC), which is the concentration where there is no colony growth. In a certain row, the 1st well was treated as a negative control without using any chemicals, while the 8th well was treated as a positive control using standard antibiotic azithromycin. The MIC and MBCs test of two compounds (**3** and **5**) against the five tested bacterial pathogens have been investigated for the first time.

Antifungal efficacy

The poisoned food technique²¹ was employed to explore the *in vitro* antifungal efficacy, using potato dextrose agar (PDA) as the culture medium. A necessary amount of medium was taken in a conical flask separately and was sterilized in an autoclave for 15 min. After autoclaving, a weighed amount of the test chemical (2% in DMSO) was added to the sterilized medium in a conical flask at the point of pouring to obtain the desired concentration. The sterilized melted PDA (at 45 °C) was poured into each Petri dish (90 mm) at the rate of 15 mL. The small portions of the mycelium of each fungus were placed carefully at the center of the semi-solid PDA medium of each plate with the help of sterilized needles. The experimental dish was incubated at 37 °C and after 48 h. The percentage of inhibition of mycelial growth of the test fungi was calculated by using the following equation:

$$I = \frac{C-T}{C} \times 100 \quad (1)$$

where I = percentage of inhibition, C = diameter of the fungal colony in control (DMSO), T = diameter of the fungal colony in treatment.

A positive control was maintained with standard antibiotic nystatin and a negative control was also maintained without using any compounds. The averages of three measurements were considered as the radial mycelia growth of the fungus in mm.

Computational details

PASS parameter prediction

The online web application PASS (<http://www.pharmaexpert.ru/passonline/>) has been employed to calculate the antimicrobial activity

spectrum of the selected MDM derivatives.²² Firstly, the structures of the MDM derivatives were drawn, and then changed into their SMILES formats by using the SwissADME free online applications (<http://www.swissadme.ch>), which are renowned for determining antimicrobial spectra using the PASS web tool. This server is planned to surmise above 4000 types of antimicrobial function, together with drug and non-drug activity, which helps to suggest the best potential objects with 90% validity. PASS outcomes are revealed by Pa (probability for active molecule) and Pi (probability for inactive molecule). Having potentialities, the Pa and Pi scores vary in the range from 0.00 to 1.00, and usually, Pa \geq Pi \geq 1, as these potentialities are predicted freely. The biological actions with Pa > Pi are only thought of as probable for a selected drug molecule. PASS calculation outcomes were explained and used flexibly, *viz.* (i) when Pa is greater than 0.7, the probability to identify the activity is analytically high, (ii) if 0.5 < Pa < 0.7, the probability to identify the activity is analytically low, again, the molecule is perhaps not so alike to well-conversant pharmaceutically used drugs and (iii) if Pa < 0.5, the potentiality to identify the activity analytically is even lower. As a result, the prediction of the spectrum of the antimicrobial activity of a probable drug molecule is expressed as its intrinsic parameter.

Antiviral activities evaluation

Antiviral molecules (AVMs) are a particular category of antimicrobial drugs employed for the treatment of viral infections by inhibiting the growth of the viral pathogen(s) inside the host cell. For antiviral activity calculation, we used online software (<http://crdd.osdd.net/servers/avcpred>), which exhibited inhibitory percentage. The SD file format of the MDM derivatives was input for predictions. The assessment was performed for the development of antiviral therapeutics and also to suggest the best inhibitory MDM derivatives for future research.

Designing and optimization

In computer-based drug design, the calculation of thermal, molecular orbitals, and molecular electrostatic features is widely performed based on quantum mechanical methods.²³ Geometrical calculation and subsequent alteration of all MDM derivatives were performed employing the Gaussian 09 program.²⁴ Optimization and calculation of the thermal and molecular orbital properties of all the MDM derivatives were carried out by employing the density functional theory (DFT) force field with Beck's (B)²⁵ three-feature hybrid model and Lee, Yang, and Parr's (LYP)²⁶ correlation functional applying the basis set 3-21G. Gibbs free energy, dipole moment, enthalpy, heat capacity, entropy, total energy, and polarizability were enumerated for each compound. Electronic molecular orbital properties HOMO and LUMO were measured by using the same geometrical theory. The energy gap

of HOMO–LUMO, molecular hardness (η), and softness (S) were enumerated for each MDM derivatives from the energy values of electronic orbitals HOMO and LUMO, according to Parr and Pearson's explanation of DFT and Koopmans' theorem (Pearson, 1986) on the interrelation between ionization energy and electronic energy (E) with HOMO and LUMO energies (ϵ). The equations used to determine η and S were as follows:

$$\eta = \frac{[\epsilon_{\text{LUMO}} - \epsilon_{\text{HOMO}}]}{2} \quad (2)$$

$$S = \frac{1}{\eta} \quad (3)$$

Protein preparation and molecular docking

The crystal 3D format of SARS-CoV-2 main protease protein (pdb: 7BQY and 6Y84) was recuperated in the pdb from the protein data bank.²⁷ PyMol (version 1.3) software packages were employed to remove all heteroatoms and water molecules.²⁸ Energy minimization of the protein was performed by using Swiss-PdbViewer (version 4.1.0).²⁹ Furthermore, a molecular docking study against SARS-CoV-2 main protease protein 7BQY and 6Y84 was conducted on the optimized drugs. Finally, the PyRx application (version 0.8) was used to carry out molecular docking simulation,³⁰ envisaging the target protein as a

macromolecule and the MDM derivatives as a ligand. The protein and ligands were inputted by converting the pdb format to pdbqt and AutoDock Tools of the MGL software package was used to perform this job. In AutoDockVina, the size of the grid box was maintained at 48.8375, 65.6838, and 57.1841 Å (for 7BQY), and 37.0771, 63.9808, and 62.9744 Å (for 6Y84) along the X, Y, and Z axes. After docking, both the structures of the macromolecule and of the ligand were saved in pdbqt format and Accelrys Discovery Studio (version 4.1) was employed to explore the results of docking and predict the non-bonding interactions among the MDM derivatives and the amino acid chain of the receptor protein.³¹

The validation was checked by PROCHECK online server and it gives 98.88 and 97.06 overall quality factors in ERRAT (http://www.ncbi.nlm.nih.gov/entrez/query.fcgi?cmd=Retrieve&db=PubMed&list_uids=8401235&dopt=Abstract), 97.32% score in VERIFY 3D (<https://www.ncbi.nlm.nih.gov/pubmed/1853201?dopt=Abstract>). The PDBsum online server was also used to validate the main protease receptor with the Ramachandran plot (Fig. 1), which reveals 89.4% (6Y84) and 100% (7BQY) residues in the allowed region, and no residues were missed.

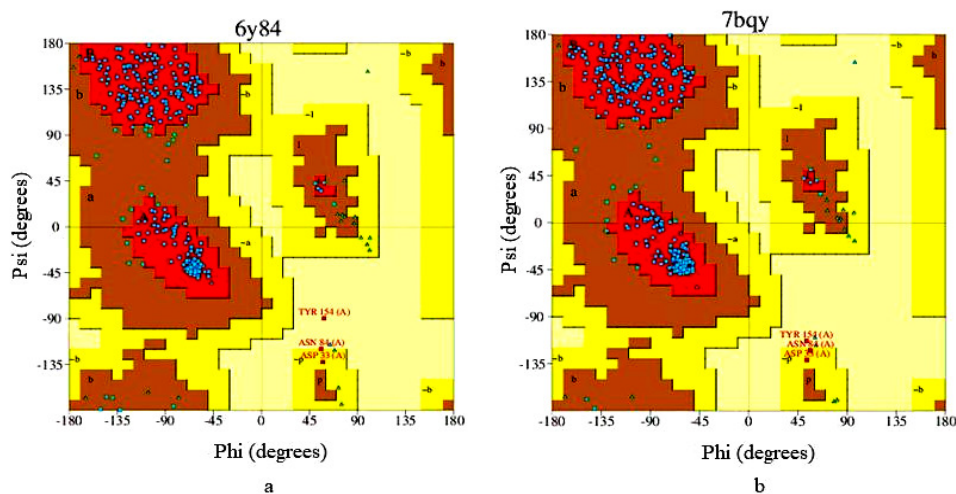


Figure 1: Ramachandran plot for the main protease (a) 6Y84 and (b) 7BQY

Pharmacokinetic prediction

The online server admetSAR was employed to calculate the pharmacokinetic properties of the designed MDM derivatives, as well as the parent compound. We accessed the online database, admetSAR, for evaluating the pharmacokinetics profile involved in drug metabolism, toxicity, and absorption of the MDM and its selected analogs.³² Using the structural resemblance exploration methodology, admetSAR foretells the latest and most widespread, manually curated results for several chemicals related to acquainted absorption, distribution, metabolism,

excretion, and toxicity (ADMET) profiles. For ADMET calculation, the admetSAR application was employed, in which 96,000 sole compounds (including 45 types of ADMET-related parameters), proteins, species, or organisms are diligently curated from various literature. Although it is quite impossible to justify all of these chemicals and to identify whether this project included carbohydrate-based drugs, well-known Pt-based drugs (cisplatin and carboplatin), and metal-based drugs approved by the Food and Drug Administration and in clinical trials were used as test candidates to verify the monosaccharide derivatives in

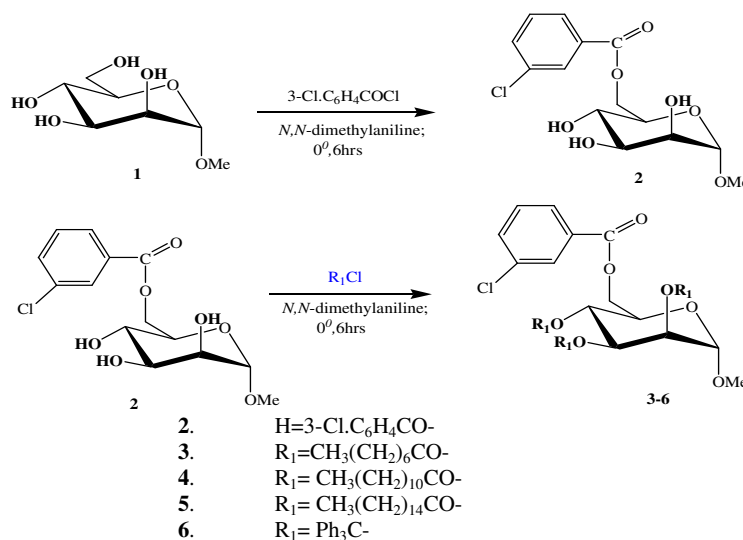
this study. Moreover, to point out probable candidates of a drug, we also calculated *in silico* parameters, which provides an insight into the pharmacokinetic features:³³ absorption in the human intestine, percolation of the blood-brain barrier, and the central nervous system (CNS), the metabolism, indicating the chemical biotransformation of a potential drug by the body, total clearance of the drugs and the toxicity levels of the selected molecules.

RESULTS AND DISCUSSION

Chemistry

The main objective of the research work presented in this paper was to carry out regioselective 3-chlorobenzoylation of methyl α -D-mannopyranoside (**1**) with 3-chlorobenzoyl chloride using the direct method (Scheme 1). A

series of derivatives of the resulting 3-chlorobenzoylation product were prepared using a wide variety of acylating agents. The 3-chlorobenzoate **2** and its derivatives (**3-6**) were employed as test compounds for antibacterial and antifungal screening studies against some human pathogenic bacteria and plant pathogenic fungi. In addition, PASS and antiviral predictions and *in silico* (quantum chemical, molecular docking, and pharmacokinetic) findings also rationalized the *in vitro* results and suggested the modified MDM derivatives are probable antimicrobial candidates, and are suitable for SARS-CoV-2 main protease protein (PDB: 7BQY and 6Y84). Figure 2 represents the whole workflow of the study.



Scheme 1: Reagents and conditions: dry C₆H₅N(CH₃)₂, -5 °C, DMAP, stirring for 6–8 h, R₁ = several acyl halides (3–

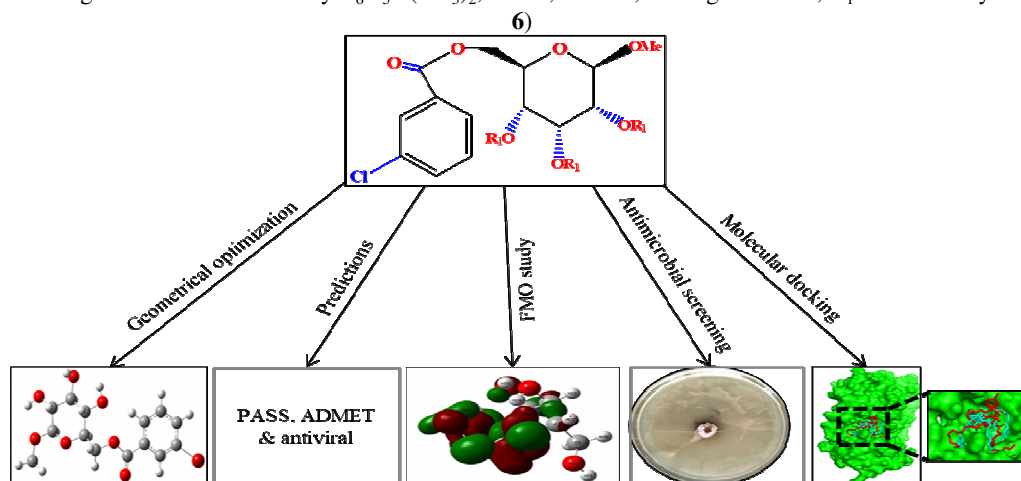


Figure 2: Schematic workflow diagram

Characterization

The MDM (**1**) was initially converted to the 3-chlorobenzoate **2** by treatment with 3-chlorobenzoyl chloride in anhydrous *N,N*-dimethylaniline (~3 mL), and DMAP by the direct method, followed by the usual workup and purification, which gave compound **2** in 88% yield, as needles, m.p. 110-112 °C. The structure of the 3-chlorobenzoate derivative **2** was established by analyzing its IR, ¹H-NMR, and mass spectra. Its IR spectrum showed absorption bands at 1689 (-CO stretching) and 3401-3469 cm⁻¹ (br) (-OH stretching), thereby suggesting the presence of hydroxyl and carbonyl groups in the molecule (Fig. 3). In its ¹H-NMR spectrum, the proton doublets at δ 8.00 (*J* 7.5 Hz) and δ 7.46 (*J* 7.7 Hz), one proton singlet at δ 7.83, and one

proton triplet at δ 7.28 (*J* 7.6 Hz) corresponded to the aromatic protons in the 3-chlorobenzoyl group (Fig. 4). The large downfield shift of C-6 to δ 5.48 (as m, 6a) and δ 4.83 (as m, 6b) suggested the introduction of the 3-chlorobenzoyl group at position 6. The structure of compound **2** was supported by the preparation of its octanoyl derivative **3**. Its IR spectrum displayed the absorption band at 1688 cm⁻¹ for C=O stretching. In its ¹H-NMR spectrum, two six-proton multiplets at δ 2.40 {3×CH₃(CH₂)₅CH₂CO-} and 1.70 {3×CH₃(CH₂)₄CH₂CH₂CO-}, a twenty four-proton multiplet at δ 1.30 {3×CH₃(CH₂)₄(CH₂)₂CO-} and nine-proton multiplet at δ 0.91 {3×CH₃(CH₂)₆CO-} were due to the presence of three octanoyl groups to the molecule.

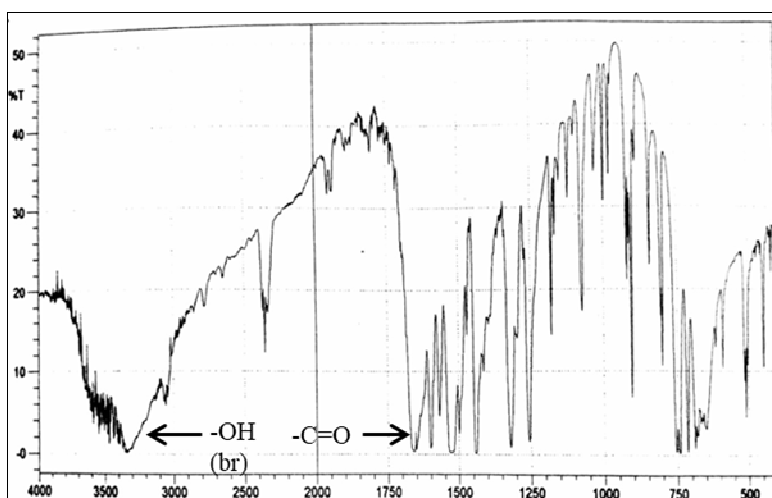


Figure 3: IR spectra of the compounds **2** and **3**

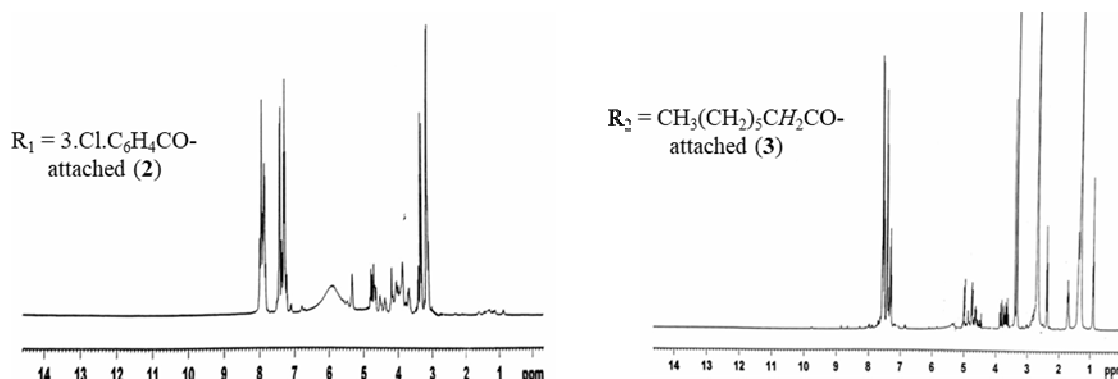


Figure 4: ¹H-NMR spectra of the compounds **2** (left) and **3** (right)

Table 1
Zone of inhibition observed against Gram-positive and Gram-negative bacteria

Compound no.	The diameter of the zone of inhibition in mm				
	Gram-negative bacteria			Gram-positive bacteria	
	<i>P. aeruginosa</i>	<i>E. coli</i>	<i>S. abony</i>	<i>S. aureus</i>	<i>B. subtilis</i>
1	--	2±0.1	--	3±0.1	--
2	NI	13±0.1	NI	*15±0.2	10±0.1
3	11±0.1	*15±0.2	11±0.1	11±0.1	*18±0.2
4	NI	NI	14±0.1	*20±0.3	*25±0.4
5	*19±0.1	*18±0.1	11±0.1	11±0.1	*20±0.3
6	NI	NI	NI	12±0.1	9±0.1
Azithromycin	**19±0.2	**18±0.2	**17±0.2	**19±0.2	**17±0.2

Data are presented as mean ± SD, and values are averages of triplicate experiments. Statistically significant inhibition ($p < 0.05$) is marked with an asterisk (*) for test compounds and a double asterisk (**) for the reference antibiotic azithromycin; NI = no inhibition

The structure of the 3-chlorobenzoate (**2**) was finally confirmed by its conversion into the lauroyl (**4**), palmitoyl (**5**), and trityl (**6**) derivatives. In the ¹H-NMR spectrum of compound **4**, two six-proton multiplets at δ 2.34 {3×CH₃(CH₂)₉CH₂CO-}, δ 1.70 {3×CH₃(CH₂)₈CH₂CH₂CO-}, a forty eight-proton multiplet at δ 1.28 {3×CH₃(CH₂)₈(CH₂)₂CO-} and a nine-proton multiplet at δ 0.90 {3×CH₃(CH₂)₁₀CO-} indicated the presence of three lauroyl groups. Its conversion to palmitoyl derivative (**5**), and trityloate (**6**) and their identification further supported the structure of the 3-chlorobenzoate derivative (**2**). Thus, selective 3-chlorobenzoylation of methyl α -D-mannopyranoside (**1**), using the direct acylation method was unique because all the reactions provided single-crystalline derivatives in good yields.

Antibacterial evaluation

The results of antibacterial activity of the test compounds (MDM derivatives) (**2-6**) were measured in terms of zone of inhibition and are presented in Table 1. The compounds showed promising inhibitory activity against a number of both Gram-positive and Gram-negative bacteria. The inhibition data indicated that compound **4** was more active (25±0.4 mm) against *B. subtilis* than the standard antibiotic (17±0.2 mm), also showing the highest activity against these bacteria amongst all the others investigated (Table 1). On the other hand, compound **4** also showed more activity against *S. aureus* and *B. subtilis* than the standard drug. However, compounds **3** and **5** were also crucially active against all the five tested organisms. The screening data suggest that

compound **5** showed excellent inhibition against both *P. aeruginosa* and *E. coli* bacteria. From the results, it was also observed that compounds **3** and **5** were very effective against all the tested pathogens, as compared to the standard antibiotic, which prompted us to carry out the MIC and MBC tests for these compounds, and the results are presented in Table 3. Besides, based on the response against the pathogens, the compounds can be ordered as **5**>**3**>**4**>**2**>**6**>**1**. We also observed that some compounds, such as **3**, **4**, and **5**, are active against both Gram-positive and Gram-negative organisms. Thus, these compounds may be targeted for future studies for their usage as broad-spectrum antibiotics.

MIC and MBC assays

MIC and MBC methods are widely used in the comparative testing of new agents. The compounds that had greater zones of inhibition, *i.e.* compounds **3** and **5**, were subjected to tests to assess their MIC and MBC activities against other commonly occurring microbes. The observed MICs of the compounds for the bacterial pathogens are listed in Table 2. The lowest value of MIC was found for compound **5** (0.3125±0.01 mg/mL) against *B. subtilis*. Whereas, the highest MIC (1.25±0.03 mg/mL) was observed for compound **5** against both *S. abony* and *S. aureus*, and compound **3** against *P. aeruginosa*, *S. aureus*, and *S. abony*. Besides, compound **3** demonstrated a MIC value of 0.625±0.02 mg/mL against *B. subtilis* and *E. coli*, and compound **5** exhibited the same MIC value against *P. aeruginosa* and *E. coli*. Furthermore, based on the MBC data in Table 3, compounds **3** and **5** killed above 99.0% organisms of all the tested pathogens, and showed

the highest MBC value of 2.50 ± 0.05 mg/mL. The lowest value of MBC was found for compound **5**

(0.625 ± 0.02 mg/mL), against *B. subtilis*.

Table 2
MIC values of the compounds against tested organisms

Compound no.	MIC values in mg/mL				
	Gram-negative bacteria			Gram-positive bacteria	
	<i>P. aeruginosa</i>	<i>E. coli</i>	<i>S. abony</i>	<i>S. aureus</i>	<i>B. subtilis</i>
3	1.25 ± 0.03	0.625 ± 0.02	1.25 ± 0.03	1.25 ± 0.03	0.625 ± 0.02
5	0.625 ± 0.02	0.625 ± 0.02	1.25 ± 0.03	1.250 ± 0.03	0.312 ± 0.01

Table 3
MBC values of the compounds against tested organisms

Compound no.	MBC values in mg/mL				
	Gram-negative bacteria			Gram-positive bacteria	
	<i>P. aeruginosa</i>	<i>E. coli</i>	<i>S. abony</i>	<i>S. aureus</i>	<i>B. subtilis</i>
3	2.50 ± 0.05	1.25 ± 0.03	2.50 ± 0.05	2.50 ± 0.05	1.25 ± 0.03
5	1.25 ± 0.03	1.25 ± 0.03	2.50 ± 0.05	2.50 ± 0.05	0.625 ± 0.02

Table 4
Antifungal activities of the synthesized compounds

Compound no.	% Inhibition of fungal mycelial growth	
	<i>Aspergillus niger</i>	<i>Aspergillus flavus</i>
1	NI	NI ± 0.5
2	58 ± 0.1	$*61 \pm 0.1$
3	$*62 \pm 0.2$	$*62 \pm 0.3$
4	$*70 \pm 0.5$	55 ± 0.5
5	$*82 \pm 1.0$	44 ± 0.2
6	$*79 \pm 1.0$	NI
Nystatin	$**66 \pm 0.5$	$**63 \pm 0.5$

Data are presented as mean \pm SD and values are averages of triplicate experiments. Statistically significant inhibition ($p < 0.05$) is marked with an asterisk (*) for test compounds and a double asterisk (**) for the reference antibiotic azithromycin; NI = No inhibition

Antifungal efficacy

It was also observed from the antifungal screening data that the compounds **4** ($70 \pm 0.5\%$), **5** ($82 \pm 1.0\%$), and **6** ($79 \pm 1.0\%$) showed the highest toxicities against *A. niger*, even higher than a standard antibiotic, nystatin ($66 \pm 0.5\%$). However, the inhibition of mycelial growth exhibited by the compound **2** ($58 \pm 0.1\%$) against *A. niger* and compounds **2** ($61 \pm 0.1\%$), **3** ($62 \pm 0.3\%$), and **4** ($55 \pm 0.5\%$) against *A. flavus* were reasonably high, though not as high as that of the standard antibiotic. These antifungal results are presented in Table 4. The results of the present investigation showed that some of the newly synthesized acylated derivatives may possess a wide range of antimicrobial activities.

PASS analysis

We have predicted the antimicrobial spectra of all the MDM derivatives **2–6**, applying the PASS web server (<http://www.pharmaexpert.ru/passonline/>). The PASS results were yclept, as Pa and Pi, which are displayed in Table 5. The predictions for MDM derivatives **2–6** in Table 5 showed $0.45 < Pa < 0.48$ for antibacterial activity, $0.55 < Pa < 0.66$ for antifungal activity, $0.51 < Pa < 0.54$ for antiviral activity. These results revealed that these molecules were more efficient against viruses and fungi, in comparison with bacterial pathogens. The attachment of additional aliphatic acyl chains (C8 to C16) increased the antifungal activity (Pa $\frac{1}{4}$ 0.628) of MDM (1, Pa $\frac{1}{4}$ 0.669), whereas the insertion of $-Cl$ -benzoyl and phenyl substituted aromatic groups did not

improve it reasonably. The same scenario was observed for the antiviral and antioxidant activities, as acyl chain derivatives (**3-5**) revealed better values than halo-benzoyl derivatives (**2**) and phenyl derivatives (**6**). Significantly, the antibacterial and antiviral properties of MDM derivatives with saturated acyl chains (**3-5**) were found more promising than those of the halo-benzoyl derivatives (**2**) and phenyl derivatives (**6**), comparing also with the standard drugs azithromycin and nystatin.¹⁶⁻¹⁷

Cell-line cytotoxicity (CLC) prediction

Web-based PASS (http://www.pharmaexpert.ru/PASSonline/index.php) was used to predict the cell-line cytotoxicity of the modified MDM derivatives. Their activity against lung adenocarcinoma, non-small cell lung cancer (stage-3), and pancreatic carcinoma has been predicted to suggest the maximum nontoxic bioactive drug molecule. It was evident from the prediction in Table 6 that MDM derivatives **2-6** showed activities of $0.61 < Pa < 0.63$ for lung adenocarcinoma, $0.56 < Pa < 0.64$ for lung carcinoma and $0.58 < Pa < 0.61$ for pancreatic carcinoma. It is clear from the predicted data that

these molecules have almost equal potentiality to work against these three cancer cells.

Although all acyl chain substituted compounds (**3-5**) exhibited promising results than the triphenyl substituted (**6**), 3-chlorobenzoyl substituted (**2**). We hope to conduct such studies for the more drug-related validation of these promising MDM derivatives.

Antiviral activity prediction

After finding considerable antimicrobial and anti-carcinogenic activity, we decided to predict the antiviral activities of these carbohydrate derivatives **2-6**, and compared them with Azidothymidine (AZT, antiviral drug) and Remdesivir (COVID-19 drug) using an antiviral application (Table 7).³⁴

The predicted antiviral activities revealed that the modified MDM derivatives (**2-6**) have potential antiviral efficacy in comparison with their parent molecule. The 3-chlorobenzoyl derivatives (**2**) and phenyl derivatives (**6**) exhibited promising scores, compared to aliphatic derivatives (**3-5**), along with standard drugs Remdesivir and Azidothymidine (AZT).

Table 5
Predicted biological activity of MDM derivatives using PASS software

Compound no.	Biological Activity					
	Antibacterial		Antifungal		Antiviral	
	Pa	Pi	Pa	Pi	Pa	Pi
1	0.541	0.013	0.628	0.016	0.403	0.014
2	0.461	0.020	0.633	0.015	0.524	0.019
3	0.461	0.020	0.633	0.015	0.524	0.019
4	0.484	0.018	0.669	0.012	0.543	0.057
5	0.484	0.018	0.669	0.012	0.543	0.057
6	0.451	0.043	0.552	0.023	0.513	0.012
Azithromycin	0.964	0.000	0.723	0.009	0.517	0.008
Nystatin	0.967	0.000	0.986	0.000	0.210	0.087

Table 6
Cell-line cytotoxicity (CLC) prediction of MDM derivatives

Drug	Cancer cell line prediction result					
	Lung (Adenocarcinoma)		Lung (Carcinoma)		Pancreas (Carcinoma)	
	Pa	Pi	Pa	Pi	Pa	Pi
1	0.713	0.006	0.541	0.048	0.564	0.043
2	0.613	0.018	0.629	0.017	0.604	0.014
3	0.634	0.015	0.644	0.011	0.619	0.006
4	0.634	0.015	0.644	0.011	0.619	0.006
5	0.634	0.015	0.644	0.011	0.619	0.006
6	0.613	0.018	0.567	0.024	0.584	0.049

Table 7
Predicted antiviral activities (% inhibition) of MDM derivatives **1-6**, Remdesivir and AZT

Compound no.	General	HBV	HCV	HHV	HIV
1	-	-	-	-	-
2	39.009	21.094	27.065	44.523	60.328
3	50.288	22.169	13.042	31.19	58.523
4	51.833	22.393	13.039	30.201	59.006
5	53.323	22.543	13.039	29.227	59.483
6	55.219	24.011	14.754	31.269	61.842
Remdesivir	48.642	22.443	66.968	36.291	69.503
AZT	87.038	19.619	24.962	28.728	92.855

HBV = Hepatitis B virus; HCV = Hepatitis C virus; HHV = Human herpes virus; HIV = Human immunodeficiency virus

Table 8
Molecular formula, electronic energy, enthalpy, Gibbs free energy in Hartree and dipole moment (Debye) of MDM derivatives

Compound no.	Molecular formula	Electronic energy	Enthalpy	Gibbs free energy	Dipole moment
1	C ₇ H ₁₄ O ₆	-722.2093	-722.2084	-722.2608	4.7712
2	C ₁₄ H ₂₃ O ₇ Cl	-1520.2398	-1520.2388	-1520.3130	3.3582
3	C ₃₈ H ₆₅ O ₁₀ Cl	-2680.6903	-2680.6893	-2680.8442	4.7864
4	C ₅₀ H ₈₉ O ₁₀ Cl	-3213.7753	-3213.7744	-3213.9065	5.8436
5	C ₆₂ H ₁₁₃ O ₁₀ Cl	-3054.2954	-3054.2931	-3054.5781	4.3428
6	C ₇₁ H ₆₅ O ₇ Cl	-3891.2291	-3891.2267	-3891.2304	3.7465

Thermodynamic calculation

A general modification of chemical formation markedly influences the structural characteristics, including thermochemical and frontier molecular orbital properties. The spontaneity of a chemical reaction and reactivity of a compound can be calculated from the Gibbs free energy and enthalpy scores.^{13,15,18,35} Higher negative scores are more suitable for thermochemical stability. Additionally, in drug designing, the formation of hydrogen bonds and nonbonded interactions are impacted by the dipole moment. A higher dipole moment can enhance the binding property.³⁶ The highest free energy was (-3891.2304 Hartree) found for compound **6**, which also exhibited the best enthalpy (-3891.2267 Hartree) and electronic energy (-3891.2291 Hartree). The highest dipole moment score (5.8436 Debye) was observed for compound **5**, whereas compound **2** exhibited the lowest value (3.3582 Debye) (Table 8). So, this proved that the modification of hydroxyl (-OH) groups of MDM significantly increased their thermodynamic parameters, which indicated the inherent stability of the synthesized derivatives.

The physicochemical and thermophysical data reported in Table 9 allowed identifying that the compound **6**, having higher molecular weight (1064.50 g/mol), displayed the best value for

polarizability (498.1964 a.u.) among all the synthesized derivatives. However, the highest values of heat capacity (309.642 cal/mol-kelvin) and entropy (425.076 cal/mol-kelvin) were observed for compound **5**. All the aliphatic derivatives (**3-5**) revealed comparatively higher energy scores than the others. Moreover, the presence of bulky acylating groups also caused a possible improvement of polarizability. However, it could be disclosed that all the synthesized MDM derivatives may be more stable than their parent structure.

Frontier molecular orbital (FMO) analysis

The molecular orbitals are the most vital orbitals in a molecule, and they are thought to distinguish the chemical reactivity and kinetic stability. The frontier molecular orbitals are called HOMO and LUMO (Table 10).

The transition from the ground to the first excited state is associated with the electronic absorption, and it is predominantly explained by one-electron excitation from HOMO to LUMO.³⁷ Kinetic stability rises with the improvement of the HOMO-LUMO gap. As a result, the elimination of electrons from the ground state HOMO to the excited state LUMO needs more energy. Table 10 presents the calculated values of molecular orbital

energies, including the two globally known chemical factors, hardness, and softness, which were listed for all MDM derivatives. The best softness was found for compound **5**. Also, compound **5** exhibited an insignificant HOMO–LUMO gap (4.1107 eV) and hardness, revealing that the derivative is much more reactive than the others, according to Pearson.³⁸ Besides, compound **3** exhibited the highest HOMO–

LUMO gap (5.4890 eV), which was less than that of the parent structure methyl α -D-mannopyranoside (**1**) (7.5679 eV). This reveals that the stability of compound **3** was close to that of MDM (**1**). Figures 5 and 6 successively present the HOMO–LUMO distribution plot of compound **3** and the DOS plots for the highest and lowest energy gaps of the derivatives **3** and **5**.

Table 9
Molecular weight (g/mol), polarizability (a.u.), heat capacity (cal/mol-kelvin), entropy (cal/mol-kelvin) and total energy (Hartree) of MDM derivatives

Compound no.	Molecular weight	Polarizability	Heat capacity	Entropy	Total energy
1	194.18	85.3296	49.303	110.240	-722.4470
2	338.50	169.4473	78.607	156.162	-1520.5294
3	716.50	355.5086	182.246	298.280	-2033.6125
4	884.50	413.2076	231.534	341.327	-3441.2259
5	1052.5	524.9012	309.642	425.076	-4109.6642
6	1064.50	498.1964	279.369	394.607	-3891.4404

Table 10
Energy (eV) of HOMO, LUMO, energy gap, hardness and softness of MDM derivatives

Compound no.	ϵ^{HOMO}	ϵ^{LUMO}	Gap	Hardness (η)	Softness (S)
1	-6.1918	1.3761	7.5679	3.7839	0.2643
2	-6.0187	-1.6147	4.4040	2.2020	0.4541
3	-7.0740	-1.5850	5.4890	2.7445	0.3643
4	-8.7679	-3.3715	5.3964	2.6982	0.3706
5	-8.0634	-3.9527	4.1107	2.0553	0.4865
6	-8.3964	-3.0967	5.2997	2.6498	0.3773

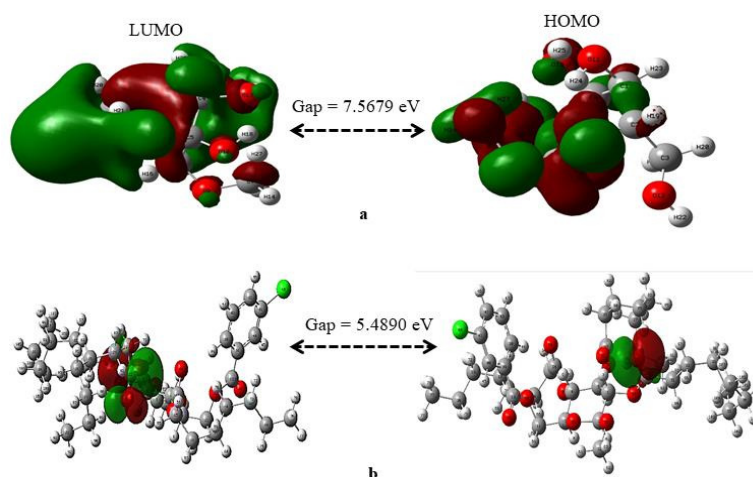


Figure 5: HOMO and LUMO distribution plots of (a) MDM and (b) its derivative **3**

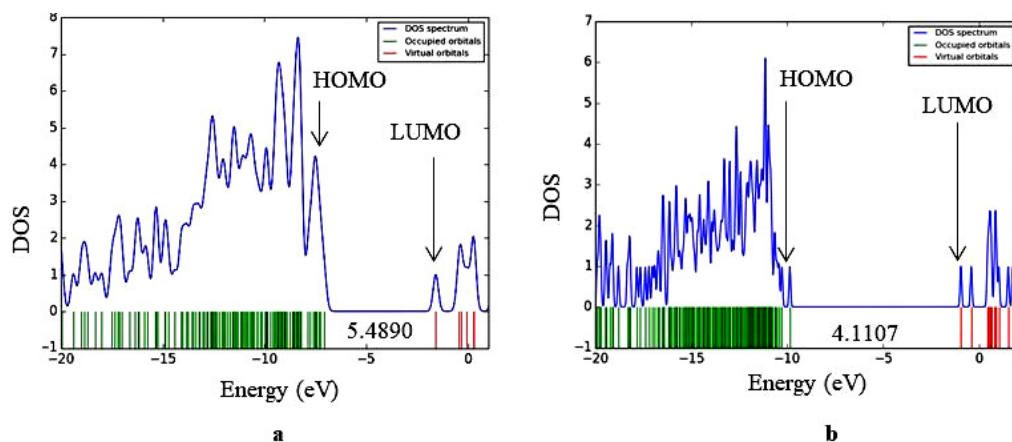


Figure 6: DOS plots of (a) compound **3** and (b) compound **5**

In Figure 5, the LUMO plot for compound **3** demonstrates that the electrons were gathered at the upper regions of the modified acylating substituents only, whereas the HOMO plot indicates that the electrons were amassed on the upper regions of the sugar ring.

Molecular electrostatic potential (MEP) surface

The MEP has gained attention as a reactivity factor displaying the most potential regions for the electrophilic and nucleophilic attack of charged point-like reagents on organic compounds.³⁹ It helps explain the biological cognizance method, as well as H-bonding interaction.⁴⁰ The map of electrostatic potential provides an easy method to predict how different geometries could interact with each other. The MEP of the selected molecule was predicted based on B3LYP with a basis set 3-21G optimized result and is displayed in Figure 7. MEP is important because it simultaneously shows a molecular shape and size with positive, negative and neutral electrostatic probable areas via color difference. It is helpful in studies of the correlation between compound structure and physicochemical parameters.⁴¹ MEP was calculated to identify the reactive zones for electrophilic and nucleophilic invasion of the optimized structure of compounds (**1**, **2**, **3** and **4**). The diverse scores of the electrostatic potential map were displayed by various colors (potential increase as per the following sequence: red < orange < yellow < green < blue). The red zone represented a spacious negative area, which exhibited a suitable zone for electrophilic invasion, the blue site indicated the best positive

zone favorable for nucleophilic interaction, and the green color represented nil probable zones.

Natural bond orbital (NBO) analysis

The partial atomic charge is essential for such purposes in molecular computations, as a simplified representation of global charge distribution in a molecule, predicting its conformational behavior. To know the charge distribution and the intrinsic property of the interactions in the designed structure, NBO analysis has been carried out. The polarity of chemical bonds often influences the structure and reactivity of a molecule.⁴² The molecular dipole moment is a vector, which does not clearly define the polarity of the molecule. Different methods have been proposed for assigning partial charges to the interacting atoms within a molecule. The approaches of Mulliken Population Analysis and Natural Bond Orbital were employed to compute the partial charges of all drugs interacting atoms.⁴³ They are the most popular analysis methods used. The dipole moment and molecular polarizability are related to atomic charges.⁴⁴ Here, all the hydrogen atoms showed positive charge by both methods, and other electronegative atoms (Cl and O) – negative charge by both methods, as expected (Fig. 8).

The compound **2** (C-2 and C-17) showed greater positive charge, due to the presence of a higher electronegative element oxygen (O-19, O-22, and O-25), and H-5 exhibited a higher positive value than the other hydrogen because of the oxygen atom of the hydroxyl group. Similarly, compound **3** (C-1, C-2, C-17 and C-28), compound **4** (C-2, C-22), and compound **5** (C-2, C-17) displayed positive charge by both methods,

due to the presence of the oxygen atom of the carbonyl group. The compound **6** (C-1) showed the highest positive charge among all the others, due to the presence of the phenyl group. As compounds **3-5** consist of aliphatic substituents, and derivatives **4** and **5** possess the longest carbon

chain, it was found that these two derivatives showed an improved result. Again, compounds **2** and **6** were modified by three aromatic rings (3-bromobenzoyl and methyl-tri-phenyl) and they exhibited almost similar results in charge distribution.

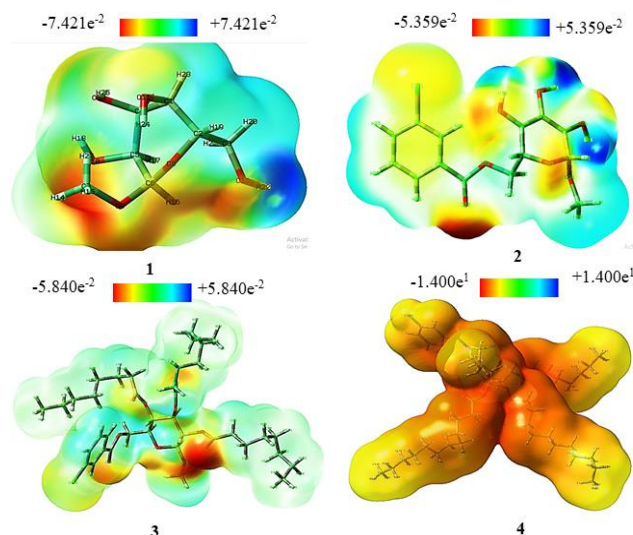


Figure 7: Map of the molecular electrostatic potential of MDM and its derivatives (**2**, **3** and **4**)

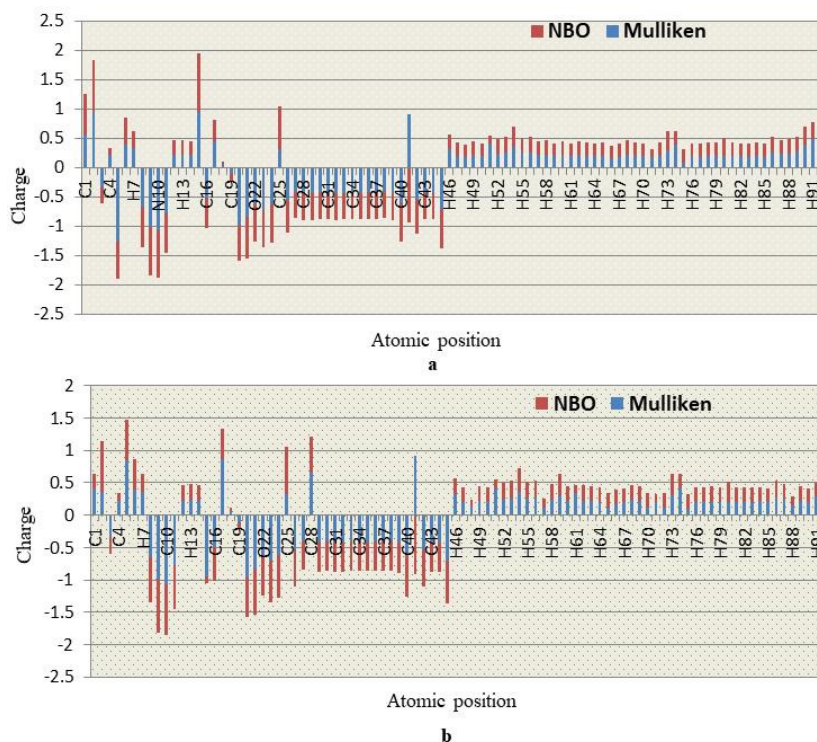


Figure 8: Partial atomic charges of (a) compound **2**, (b) and compound **3**

Finally, we depicted compounds **2** and **3** (Fig. 8) from both aliphatic and aromatic series, as these compounds exhibited a clear graphical view,

while rest of the derivatives gave a slightly scribbled view.

Molecular docking

The SARS-CoV-2 M^{pro} is one of the main enzymes in the life cycle of the virus. 2019-nCoV and SARS-CoV-2 main proteases share 94.80% of sequence identity at the amino acid level.⁴⁵ In this study, the binding mode of MDM and its derivatives against the SARS-CoV-2 main protease protein (PDB: 7BQY and 6Y84) was investigated by molecular docking analysis, particularly for the compounds with better antibacterial and antifungal activities. The analysis revealed that MDM, which was found to be inactive in antibacterial and antifungal tests, exhibited binding affinity of -5.4 and -5.1 kcal mol⁻¹ for both protease proteins, and the binding affinities of its derivatives (**2-5**) in the ascending order were as follows: (-6.7 < -7.5 < -8.1 < -8.5) kcal mol⁻¹ for 7BQY and (-6.7 < -7.8 < -8.0) for 6Y84 (Table 11).

As shown in Table 11, derivative **5** showed the highest binding affinities, compared to its parent compound, MDM. Compound **5** had three long aliphatic substituents in the MDM structure, providing a high gathering of electrons in the molecule, indicating the highest binding score (Figs. 9 and 10). These results demonstrate that the modification of the -OH group, along with a long aliphatic chain/aromatic ring molecule, increased the binding affinity, while the addition of hetero groups, like Cl, made some fluctuations in binding affinities. However, the modification with halogenated aromatic rings also increased the binding affinity. Non-bonding interactions are often used to predict the shape and behavior of molecules. Among all the non-bonding interactions, CH/O, CH/ π , NH/ π , OH/ π , and CH/N, the CH/O is the highest observed interaction found in protein-ligand docking. The parent molecule MDM exhibited interactions with the His41 and Cys145 of the proteins, as well as a

sharp interaction within a closer bond distance (2.300 Å) (Table 12).

Additionally, Gly143, Thr292, and Glu166 interactions were found, whereas Glu166 revealed a shorter distance (1.2734 Å) for 7BQY, because of the unique interaction of the branched alkyl chain with the sugar ring. Figures 11 and 12 showed that the 3-chlorobenzoyl derivative (**2**) binds firmly with both protease proteins through conventional hydrogen bonds with residues Cys145, Gly143, besides other interactions, such as carbon-hydrogen bonds (Thr26, Arg298 and Thr111), alkyl and pi-alkyl (Tyr239, Met49 and Phe294) interactions. However, a closer distance was observed for Cys145 (1.967 Å) and Thr26 (2.156 Å). Aliphatic derivatives (**3-5**) revealed some similar binding sites with residues Cys145 (shorter distance 2.159 Å), His41, Phe294, Gln110 and His164, which are also found in compound (**2**). It is clear from the structural contrast, aliphatic derivatives (**3-5**) have an additional 3-chlorobenzoyl ring substituent in the parent structure, providing high density of electrons in the molecule, leading to comparatively higher binding affinity in the case of both macromolecules.

Along with PHE294, compounds **4** and **5** displayed the maximum π - π interactions with PHE294, denoting tight binding to the active site. Reports suggest that PHE294 is considered as the principal component of PPS and PPT, responsible for the accessibility of small molecules to the active site. In both cases, the binding affinity and the binding specialty are increased in the case of compounds **2-5** due to significant hydrogen bonding. It was observed that the modifications of the -OH group of MDM (**1**) increased the π - π interactions with the residues of the active site, while increasing their polarity, which resulted in the formation of hydrogen bonding interactions.

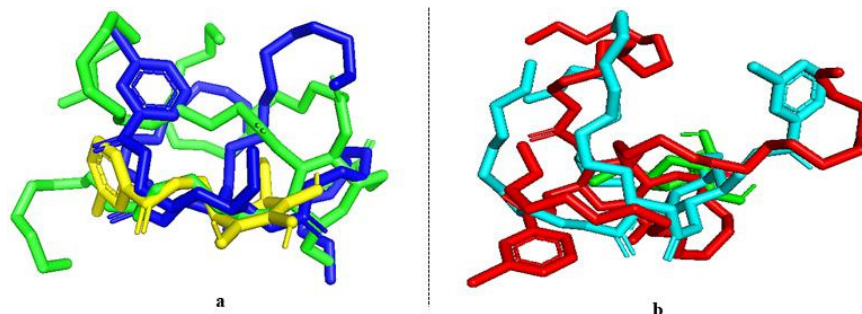


Figure 9: Superimposed face of all the ligands predicted from docking (a) 7BQY and (b) 6Y84

Table 11
Binding scores of derivatives against M^{pro} (7BQY and 6Y84)

Compound no.	Main protease 7BQY				Main protease 6Y84			
	Binding affinity	No. of hydrogen bonds	No. of hydrophobic bonds	Interaction type	Binding affinity	No. of hydrogen bonds	No. of hydrophobic bonds	Interaction type
1	-5.4	2	1	H, PPT	-5.1	3	Absent	H
2	-6.7	5	1	H, C, PA	-6.7	5	4	H, A, PA, PPT
3	-7.5	2	4	H, PPT, A	-6.0	4	5	H, C, A, PAn, PA
4	-8.1	1	5	H, A, PA, PPS	-7.8	4	4	H, A, PA, PPS
5	-8.5	1	3	H, PA, PS	-8.0	2	2	H, C, A, PS
Remdesivir	-10.5	2	2	H, A, PA	-10.3	5	1	SB, AC,

H = Conventional hydrogen bond; C = Carbon-hydrogen bond; A= alkyl; PA = Pi-alkyl; PPS = Pi-Pi stacked; PS = Pi-Sigma; PPT = Pi-Pi T-shaped

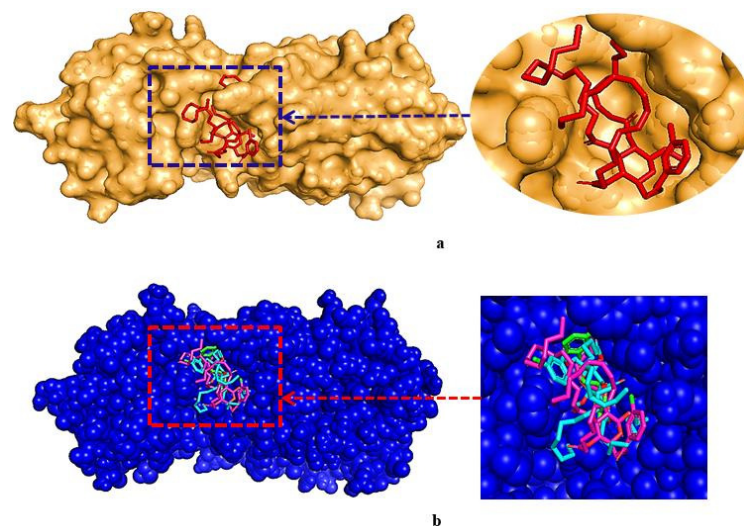


Figure 10: (a) Docked pose of derivative **5** with 7BQY; (b) 2D interaction of derivative (**3-5**) with 7BQY

Table 12
Non-bonding interactions of derivatives with amino acid residues of M^{pro} (7BQY and 6Y84)

Compound no.	Main protease 7BQY				Compound no.	Main protease 6Y84			
	Hydrogen bond		Hydrophobic bond			Hydrogen bond		Hydrophobic bond	
	Residues	Distance (Å)	Residues	Distance (Å)		Residues	Distance (Å)	Residues	Distance (Å)
1	Glu166	1.273	HIS41	2.732	1	THR292	2.169		
	Gly143	2.621				CYS145	2.300		
2	Arg298	2.543	MET49	4.005	2	GLU166	2.530	TYR239	5.309
	Cys145	1.967				CYS145	2.659	LEU272	4.890
	Thr26	2.156				ASP197	2.263	LEU287	4.733
	Thr111	2.516				GLY143	2.816	PHE294	5.297
	Arg298	3.466				THR198	2.810		
3	Cys145	2.727	TYR237	4.953	3	HIS164	2.643	GLU166	3.649
	Thr199	2.227	HIS41	4.091		THR199	2.223	LEU272	4.654
			LEU27	4.438		GLN110	2.106	CYS145	4.086
			LEU287	5.314		GLU290	2.895	TYR237	5.053
4	Asn151	3.024	PHE294	4.486	4	LEU287	3.573	HIS41	5.108
			HIS164	3.681		ASN151	2.748	ILE249	3.886
			ILE106	5.282		SER158	2.084	VAL297	5.144
			CYS160	4.086		TYR54	2.409	PHE294	4.791
			PHE294	4.997		PHE294	3.883	PHE294	4.534
			HIS41	3.985		CYS145	2.159	MET49	3.489
5	Gln110	3.487	TYR154	4.975	5	GLN110	3.398	VAL297	4.484
			PHE294	4.648		ASP295	2.334	ASP295	4.223
			CYS145	5.119		CYS145	2.698		
			HIS163	4.669		GLN110	2.268		
Remdesivir	Thr26	2.749			Remdesivir	THR111	2.203		
	Thr26	2.876				THR111	2.358		

N.B. Gly = Glycine, Tyr = Tyrosine, Cys = Cysteine, His = Histidine, Arg = Arginine, Leu = Leucine, Thr = Threonine, Ile = Isoleucine, Ser = Serine, Phe = Phenylalanine, Gln = Glutamine, Asn = Asparagine, Ala = Alanine, Glu = Glutamic acid, Asp = Aspartic acid

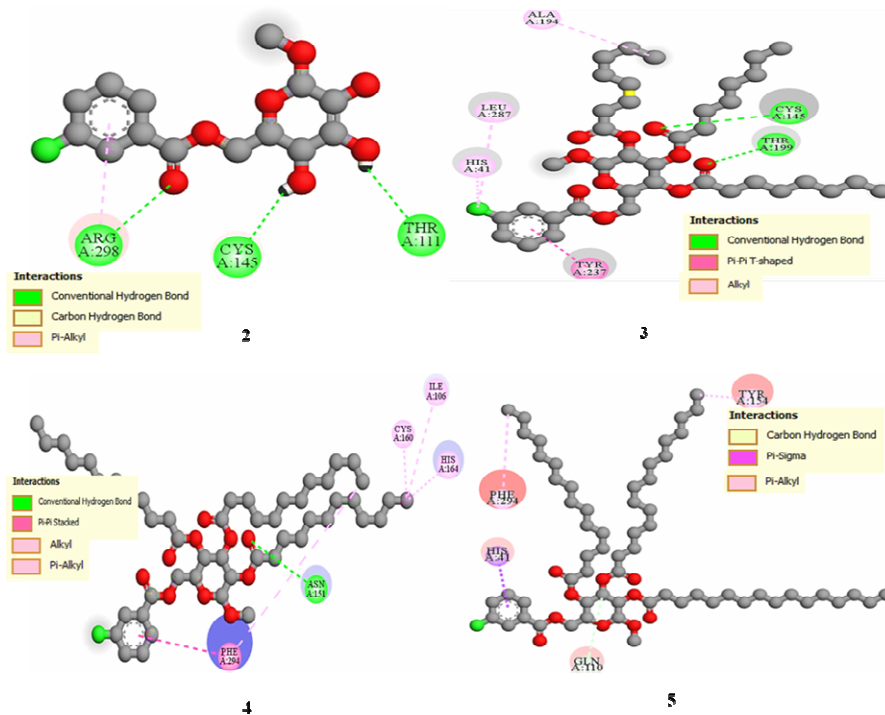


Figure 11: Non-bonding interactions of compounds 2-5 with the active site of SARS-CoV-2 7BQY performed by Discovery Studio

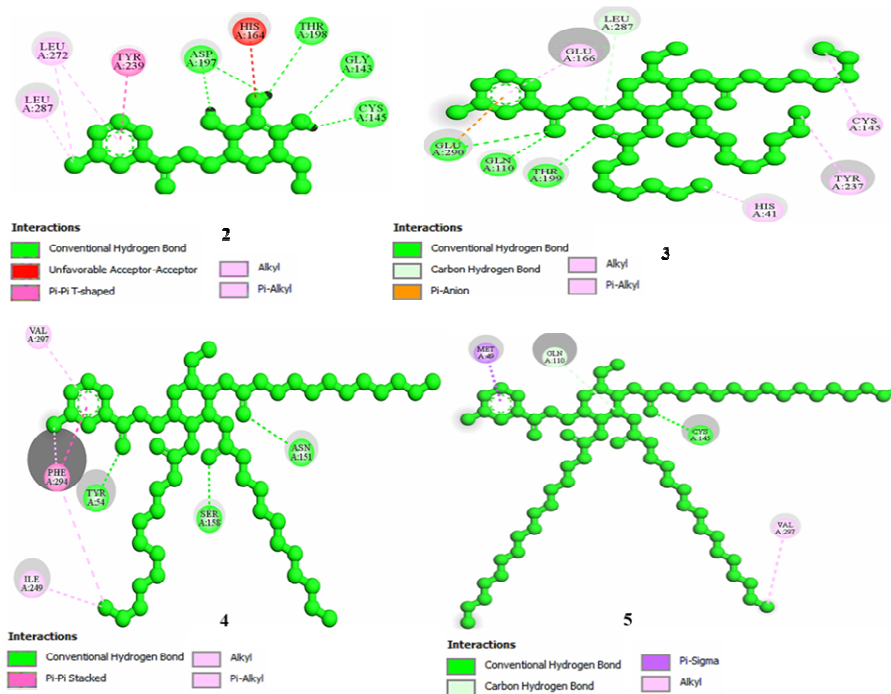


Figure 12: Non-bonding interactions of compounds 2-5 with the active site of SARS-CoV-2 6Y84 performed by Discovery Studio

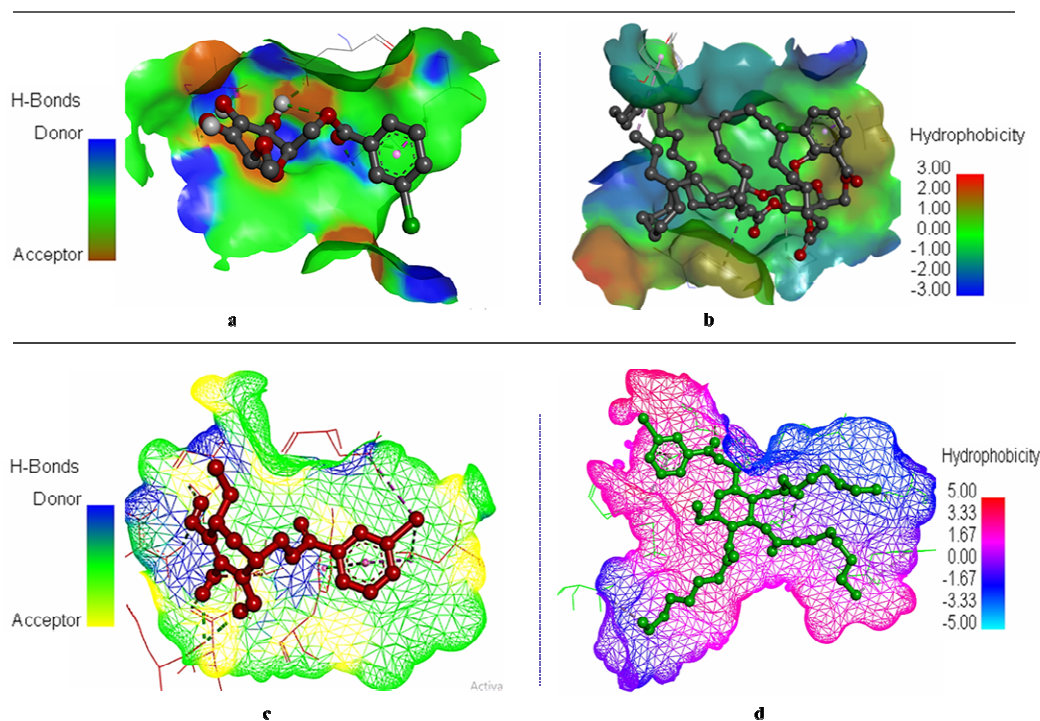


Figure 13: (a, b): Hydrogen bond and hydrophobic surface of 7BQY with compounds **2** and **5**; (c, d): Hydrogen bond and hydrophobic surface of 6Y84 with compounds **2** and **3**

The most significant H-bonds were obtained for the compounds **2** and **4**, formed with Cys145, Asn151 and Thr26 residues. It has already been reported that ten commercial medicines possibly form H-bonds with key residues of 2019-nCoV main protease.⁴⁶ H-bonds exert a vital function in shaping the specificity of ligand binding with the receptor, drug design in chemical and biological processes, and molecular recognition and biological activity. The H-bond surface and the hydrophobic surface of compounds **2**, **3** and **5** with both proteins were consequently presented in Figure 13. Although compound **9** exhibited mostly hydrogen-type non-bonding interaction, it had a significant range of hydrophobicity because of the presence of the heteroaromatic ring.

We observed from the blind docking study of all the four monosaccharide derivatives with the SARS-CoV-2 protease that the molecules are generally surrounded by the above-mentioned residues, similarly to the standard drug Remdesivir, which suggests that this molecule can prevent the viral replication of SARS-CoV-2. The distance of the ligands, along with the change in the accessible area of the two important catalytic residues (Cys145 and His41) within the active site of the protease is shown in Table 11 and Table 12. The calculated binding affinities varied in the

range from -5.4 to -8.5 kcal/mol with 7BQY, and from -5.1 to -8.0 kcal/mol with 6Y84, suggesting the molecules can spontaneously interact within the binding site of SARS-CoV-2 M^{pro}. Although the blind docking studies reveal that all the molecules can act as potential agents for COVID treatments, but from the estimated free energy of the binding values, it could be inferred that the derivative **5**, with the highest negative minimum binding energy value (-8.5 and -8.0 kcal/mol) among all the studied compounds, could be the best possible SARS-CoV-2 inhibitor. Finally, it was resolved that most of the selected monosaccharide derivatives showed promising activities and might be used to design effective antiviral drugs against SARS-CoV-2.

Pharmacokinetic prediction

All the newly modified MDM derivatives have potential activities. Therefore, to ensure that the modified compounds are viable drugs, we used the *in silico* pharmacokinetic parameters ADMET. The pkCSM online server⁴⁷ was employed to calculate the *in silico* ADMET properties (Table 13). An absorbance value below 30% indicates poor absorbance, but compounds **4-6** display a value of 100%, which reveals a good absorbance in the human intestine.

The volume of distribution (VDs) is thought high if the value is higher than 0.45. In addition, the blood brain barrier (BBB) and central nervous system (CNS) permeability standard values are as follows: >0.3 to < -1 Log BB, and > -2 to < -3 Log PS, respectively. For a given compound, a Log BB < -1 means poor distribution to brain, while Log BB >0.3 indicates potential to cross BBB, and LogPS > -2 is considered to penetrate the CNS, while Log PS < -3 means it is difficult to move in the CNS.⁴⁸ It was observed that the compounds **4-6** have the most significant potential to cross the barriers, in comparison with the standard drugs azithromycin and nystatin. Compounds **2-6** are a CYP3A4 enzyme substrate, while parent (**1**) is non-substrate for this enzyme. The enzymatic metabolism ensures the chemical biotransformation of a designed drug in the body, which plays a key role in the transformation of drug compounds. In the body, drugs produce several enzymatic metabolites, which play a role in catalyzing the reaction with several drug concentrations.⁴⁹ It is essential to consider the metabolism of drugs, which may show several physicochemical and pharmacological parameters. The cytochrome P450 (CYP450) plays a major role in drug metabolism because the major liver enzyme system is involved in phase I metabolism. Some selective CYP genes CYP1, CYP2, CYP3 and CYP4 families are found to be involved in drug metabolism, with CYP (1A2, 2C19, 2D6 and 3A4) causing the biotransformation of more than 90% of drugs undergoing phase I metabolism (Table 14). Clearance is a constant that indicates the

relationship between drug concentration in the body and the rate of elimination of the drug.

To enhance the predictions of drug likeness,⁵⁰ Ghose, Veber, Egan and Muegge filters have been used in the study (Table 15). Also, Pan-assay interference compounds (PAINS) revealed no violation with these MDM derivatives. PAINS are chemical compounds that often give false positive results in high-throughput screens. PAINS tend to react non-specifically with numerous biological targets, rather than specifically affecting one desired target. Therefore, all the synthesized compounds show a somewhat standard value and acceptable in persistence of the drug in the body. Moreover, it is necessary to examine whether the predicted compounds are non-toxic, because this plays a critical role in the selection of drugs.

The compounds designed were evaluated for their synthetic accessibility, the synthetic accessibility values for all the compounds is about 4.19 to 8.91, so, they are easy to synthesize. Specifically, the new compounds **3-6**, with a bioavailability score of 0.55, are the compounds that satisfied all the rules used to predict drug likeness. Toxicity prediction (Table 16) exhibited that none of the molecules are mutagenic or carcinogenic. Every derivative is hepatotoxic if administered above the prescribed limits. All the compounds, as well as the parent molecules, are AMES non-toxic. Lethal doses (LD50) of all the synthetic compounds were comparatively higher than the natural value. None of these compounds exhibit skin sensitization. Finally, the new molecules designed present good pharmacokinetic properties.

Table 13
Predicted *in silico* ADMET properties of MDM and its derivatives

Compound no.	Absorption			Distribution		Metabolism	Excretion
	Caco-2	HIA	P-gpI	BBB	CNS	CYP3A4 substrate	Total clearance
1	-0.893	32.866	No	-0.881	-4.67	No	0.686
2	-0.753	51.009	Yes	-1.004	-4.201	Yes	0.392
3	1.002	95.111	Yes	-2.102	-2.111	Yes	0.687
4	0.857	100.000	Yes	0.364	-1.947	Yes	1.069
5	0.713	100.000	Yes	0.622	-1.807	Yes	1.451
6	0.554	100.000	Yes	1.465	-3.349	Yes	0.010
Azithromycin	-0.211	45.808	Yes	-1.857	-3.777	Yes	-0.424
Nystatin	-0.868	0.00	No	-2.09	3.702	No	-1.357

Caco-2 permeability (log Papp in 10⁻⁶ cm/s, >0.90 indicates high permeability); HIA: Human intestinal absorption (% absorbed, $>30\%$ is better absorbed); P-gpI: P-glycoprotein inhibitor; BBB (blood brain barrier) is expressed in logBB (logBB >-1.0 moderately crosses the blood brain barrier); CNS (central nervous system) is expressed as logPS (logPS >-2.0 can easily penetrate the CNS); Total clearance is expressed in log mL/min/kg

Table 14
Drug likeness properties of MDM and its derivatives

Compound no.	Molar refractivity (Å)	Log $P_{o/w}$ (XLOGP3)	NRB	NHA	NHD	CYP3A4	CYP2D6	CYP2C9	CYP1A2	CYPC19
1	40.47	-2.65	2	6	4	No	No	No	No	No
2	75.111	0.26	5	7	3	No	No	No	No	No
3	190.85	10.96	29	10	0	Yes	No	No	No	No
4	248.54	17.46	41	10	0	Yes	No	No	No	No
5	306.22	23.96	53	10	0	No	No	No	No	No
6	309.34	15.89	20	7	0	No	No	No	No	No
Azithromycin	200.78	4.02	7	14	5	No	No	No	No	No
Nystatin	239.53	-0.20	3	18	12	No	No	No	No	No

NRB = No. of rotatable bonds; NHA = No. of hydrogen bond acceptors; NHD = No. of hydrogen bond donors

Table 15
Swiss-ADME properties of MDM and its derivatives

Compound no.	Lipinski	Muegge	Veber	Egan	Ghose	SA	BS	PAINS	TPSA (Å ²)	Csp3
1	Yes	No	Yes	Yes	No	4.30	0.55	0	99.38	1.00
2	Yes	Yes	Yes	Yes	Yes	4.19	0.55	0	105.45	0.50
3	No	No	No	No	No	6.92	0.17	0	123.66	0.74
4	No	No	No	No	No	8.52	0.17	0	123.66	0.80
5	No	No	No	No	No	10.00	0.17	0	123.66	0.84
6	No	No	No	No	No	8.53	0.17	0	72.45	0.14
Azithromycin	No	No	No	No	No	8.91	0.17	0	108.08	0.97
Nystatin	No	No	No	No	No	10.00	0.17	0	319.61	0.70

SA = Synthetic accessibility; BS = Bioavailability score; PAINS = Pan-assay interference compounds; TPSA = Topological polar surface area

Table 16
 Predicted toxicity properties of MDM and its derivatives

Compound no.	AMES toxicity	Carcinogenicity	HT	TP	RaT	AT	hERG	Skin sensitization
1	No	No	No	0.285	1.533	III	No	No
2	No	No	Yes	0.285	2.652	III	No	No
3	No	No	No	0.285	2.282	III	No	No
4	No	No	No	0.285	2.393	III	Yes	No
5	No	No	No	0.285	2.468	III	Yes	No
6	No	No	No	0.285	2.482	III	Yes	No
Azithromycin	No	No	Yes	0.285	2.769	III	No	No
Nystatin	No	No	No	0.285	2.518	III	No	No

HT = Hepatotoxicity; TP = *Tetrahymena pyriformis* toxicity pIGC50, mg/L; RaT = Rat acute toxicity LD50, mol/kg; AT = Acute oral toxicity

CONCLUSION

In this extensive study, several test compounds exhibited promising antimicrobial activity. Better inhibitory activity was observed against Gram-negative bacteria, compared to Gram-positive bacteria. Hence, the acylated derivatives of MDM (2–6) may be thought of as a possible source for the development of newer and better antimicrobial candidates against several pathogenic organisms. A few computational studies on the MDM derivatives have been attempted earlier. In the computational investigation, the most crucial parameters for chemical stability and reactivity, biological chemistry, and frontier molecular orbital study were optimized, indicating that the developed compounds were promising drug molecules. PASS prediction of the MDM derivatives 2–6 showed values of $0.45 < Pa < 0.48$ for antibacterial activity, $0.55 < Pa < 0.66$ for antifungal activity and $0.51 < Pa < 0.54$ for antiviral activity, which revealed the antimicrobial potency of the modified derivatives. Additionally, the docked complex of derivatives 2-5 and SARS-CoV-2 M^{pro} (7BQY and 6Y84) exhibited comparatively better binding scores, with significant non-bonding interactions, than the parent ligand. The ADMET calculation has shown promising results for *in silico* properties, which revealed that all the modified derivatives have an improved pharmacokinetic profile. As these compounds exhibited antibacterial and antifungal properties, they have the potential to exert antiviral effects as well. This piece of work may be helpful to assess the chemical, thermal, biological, physicochemical, and pharmacological parameters of MDM derivatives.

ACKNOWLEDGEMENTS: The authors are grateful to the Ministry of Science and Technology (MOST), Government of Bangladesh, for providing financial support to carry out this research [Ref: 39.00.0000.009.06.009.20-1331/Phy's-530, dated: 8-12-2020]. The authors are grateful to the Director of the Wazed Miah Science Research Centre, JU, Dhaka, Bangladesh, for recording the spectra.

REFERENCES

- C. R. Bertozzi and L. L. Kiessling, *Science*, **291**, 2357 (2001), <https://doi.org/10.1126/science.1059820>
- Y. Fujii, N. Dohmae, K. Takio, S. M. A. Kawsar, R. Matsumoto *et al.*, *J. Biol. Chem.*, **287**, 44772 (2012), <https://doi.org/10.1074/jbc.M112.418012>
- A. Varki, *Glycobiology*, **3**, 97 (1993), <https://doi.org/10.1093/glycob/3.2.97>
- S. M. A. Kawsar, A. K. M. S. Kabir, M. M. R. Bhuiyan, M. K. Hossain and M. N. Anwar, *J. Pharm. Sci.*, **2**, 107 (2012), <https://doi.org/10.5530/rjps.2012.3.12>
- M. Arifuzzaman, M. M. Islam, M. M. Rahman, A. R. Mohammad and S. M. A. Kawsar, *ACTA Pharm. Sci.*, **56**, 22 (2018), <https://doi.org/10.23893/1307-2080.APS.05622>
- S. M. A. Kawsar, A. A. Hamida, A. U. Sheikh, M. K. Hossain, A. C. Shagir *et al.*, *Int. J. Org. Chem.*, **5**, 232 (2015), <https://doi.org/10.4236/ijoc.2015.54023>
- S. M. A. Kawsar, M. O. Faruk, M. S. Rahman, Y. Fujii and Y. Ozeki, *Scientia Pharm.*, **82**, 1 (2014), <https://doi.org/10.3797/scipharm.1308-03>
- K. M. Rana, J. Ferdous, A. Hosen and S. M. A. Kawsar, *J. Siberian Fed. Univ. Chem.*, **13**, 465 (2020), <https://doi.org/10.17516/1998-2836-0199>
- M. M. H. Misbah, J. Ferdous, M. Z. H. Bulbul, T. S. Chowdhury, S. Dey *et al.*, *Int. J. Biosci.*, **16**, 299 (2020), <http://dx.doi.org/10.12692/ijb/16.4.299-309>

- ¹⁰ M. Z. H. Bulbul, T. S. Chowdhury, M. M. H. Misbah, J. Ferdous, S. Dey *et al.*, *Pharmacia*, **68**, 23 (2021), <https://doi.org/10.3897/pharmacia.68.e56543>
- ¹¹ M. Islam, M. Arifuzzaman, M. Rahman, M. A. Rahman and S. M. A. Kawsar, *Hacettepe J. Biol. Chem.*, **47**, 153 (2019), <https://doi.org/10.15671/hjbc.622038>
- ¹² S. R. Devi, S. Jesmin, M. Rahman, M. A. Manchur, Y. Fujii *et al.*, *Acta Pharm. Sci.*, **57**, 47 (2019), <https://doi.org/10.23893/1307-2080.APS.05704>
- ¹³ S. M. A. Kawsar, M. A. Hosen, Y. Fujii, Y. Ozeki, *J. Comput. Chem. Mol. Model.*, **4**, 452 (2020), <http://www.dx.doi.org/10.25177/JCCMM.4.4.RA.10663>
- ¹⁴ H. Lu, *Biosci. Trends*, **14**, 69 (2020), <https://doi.org/10.5582/bst.2020.01020>
- ¹⁵ M. Z. H. Bulbul, M. A. Hosen, J. Ferdous, T. S. Chowdhury, M. M. H. Misbah *et al.*, *Int. J. New Chem.*, **8**, 88 (2021), <https://doi.org/10.22034/ijnc.2020.131337.1124>
- ¹⁶ J. Maowa, M. A. Hosen, A. Alam, K. M. Rana, Y. Fujii *et al.*, *Phys. Chem. Res.*, **9**, 385 (2021), <https://doi.org/10.22036/pcr.2021.264541.1869>
- ¹⁷ A. Alam, M. A. Hosen, A. Hosen, Y. Fujii, Y. Ozeki *et al.*, *J. Mex. Chem. Soc.*, **65**, 256 (2021), <http://dx.doi.org/10.29356/jmcs.v65i1.1464>
- ¹⁸ S. M. A. Kawsar and M. A. Hosen, *Turkish Comp. Theo. Chem.*, **4**, 59 (2020), <https://doi.org/10.33435/tcandtc.718807>
- ¹⁹ S. M. A. Kawsar, A. K. M. S. Kabir, M. M. Manik, M. K. Hossain and M. N. Anwar, *Int. J. Biosci.*, **2**, 66 (2012), <http://www.innspub.net>
- ²⁰ Clinical and Laboratory Standards Institute (CLSI). Performance Standards for Antimicrobial Disk Susceptibility Tests. 23rd Informational Supplement M100–S23, Wayne, USA, 2013
- ²¹ R. K. Grover and J. D. Moore, *Phytopathology*, **52**, 876 (1962), <https://doi.org/10.4236/jqis.2011.12006>
- ²² S. Kumaresan, V. Senthilkumar, A. Stephen and B. S. Balakumar, *World J. Pharm. Res.*, **4**, 1035 (2015)
- ²³ P. H. Seeberger and D. B. Werz, *Nature*, **446**, 1046 (2007), <https://doi:10.1038/nature05819>
- ²⁴ M. J. Frisch, G. W. Trucks, H. B. Schlegel, G. E. Scuseria, A. Robb *et al.*, Gaussian 09. Gaussian Inc, Wallingford, CT, <https://gaussian.com/g09citation/>
- ²⁵ A. D. Becke, *Phys. Rev.*, **38**, 3098 (1988), <https://doi.org/10.1103/PhysRevA.38.3098>
- ²⁶ C. Lee, W. Yang and R. G. Parr, *Phys. Rev.*, **37**, 785 (1988), <https://doi.org/10.1103/PhysRevB.37.785>
- ²⁷ H. M. Berman, J. Westbrook and Z. Feng, *Nucleic Acids Res.*, **28**, 235 (2000), <https://doi.org/10.1093/nar/28.1.235>
- ²⁸ W. L. Delano, PyMOL Molecular Graphics System, De-Lano Scientific, San Carlos, CA, USA, 2002, <http://www.pymol.org>
- ²⁹ N. Guex and M. C. Peitsch, *Electrophoresis*, **18**, 2714 (1997), <https://doi.org/10.1002/elps.1150181505>
- ³⁰ C. H. Williams (Eds.), “Chemical Biology: Methods and Protocols”, Springer, New York, USA, 2015, p. 243, <https://doi.org/10.1007/978-1-4939-2269-7>
- ³¹ Version ADS 4.0, (2017), Accelrys, San Diego, USA
- ³² F. Cheng, W. Li, Y. Zhou, J. Shen, Z. Wu *et al.*, *J. Chem. Info. Model.*, **52**, 3099 (2012), <https://doi.org/10.1021/ci300367a>
- ³³ L. L. G. Ferreira and A. D. Andricopulo, *Drug Discov. Today*, **24**, 1157 (2019), <https://doi.org/10.1016/j.drudis.2019.03.015>
- ³⁴ A. Qureshi, G. Kaur and M. Kumar, *Chem. Biol. Drug Des.*, **89**, 74 (2016), <https://doi.org/10.1111/cbdd.12834>
- ³⁵ N. Cohen and S. W. Benson, *Chem. Rev.*, **93**, 2419 (1993), <https://doi.org/10.1021/cr00023a005>
- ³⁶ E. J. Lien, Z. R. Guo and R. L. Li, *J. Pharm. Sci.*, **71**, 641 (1982), <https://doi.org/10.1002/jps.2600710611>
- ³⁷ S. Saravanan and V. Balachandran, *Spectrochim. Acta A, Mol. Biomol. Spectrosc.*, **120**, 351 (2014), <https://doi.org/10.1016/j.saa.2013.10.042>
- ³⁸ R. G. Pearson, in *Procs. The Natural Academy of Sciences of the United States of America*, 1986, vol. 83, p. 8440, <https://doi.org/10.1073/pnas.83.22.8440>
- ³⁹ M. L. Amin, *Drug Target Insights*, **7**, 27 (2013), <https://doi.org/10.4137/DTI.S12519>
- ⁴⁰ P. Politzer and J. S. Murray, *Rev. Comput. Chem.*, **2**, 273 (1991), <https://doi.org/10.1002/wcms.1326>
- ⁴¹ P. Politzer and D. G. Truhlar (Eds.), “Reactivity, Structure, Scattering, and Energetics of Organic, Inorganic, and Biological Systems”, Springer, USA, 1981, <https://www.springer.com/gp/book/9780306406577>
- ⁴² H. Heinz and U. W. Suter, *J. Phys. Chem., B*, **108**, 18341 (2004), <https://doi.org/10.1021/jp048142t>
- ⁴³ K. C. Gross, P. G. Seybold and C. M. Hadad, *Int. J. Quantum Chem.*, **90**, 445 (2002), <https://doi.org/10.1002/qua.10108>
- ⁴⁴ R. S. Mulliken, *Int. J. Chem. Phys.*, **23**, 1833 (1955), <https://doi.org/10.1063/1.1740588>
- ⁴⁵ T. Serseg, K. Benarous and M. Yousfi, *Curr. Comput. Aided Drug Des.*, <https://doi.org/10.2174/1573409916666200422075440>
- ⁴⁶ X. Liu and X. Z. Wang, *J. Genet. Genom.*, **47**, 119 (2020), <https://doi.org/10.1016/j.jgg.2020.02.001>
- ⁴⁷ D. E. V. Pires, T. L. Blundell and D. B. Ascher, *J. Med. Chem.*, **58**, 4066 (2015), <https://doi.org/10.1021/acs.jmedchem.5b00104>
- ⁴⁸ D. E. Clark, *Drug Discov. Today*, **8**, 927 (2003), [https://doi.org/10.1016/s1359-6446\(03\)02827-7](https://doi.org/10.1016/s1359-6446(03)02827-7)
- ⁴⁹ S. Kok-Yong and L. Lawrence, in “Basic Pharmacokinetic Concepts and Some Clinical Applications”, edited by Tarek A. Ahmed, InTechOpen, London, UK, 2015, <https://doi.org/10.5772/59929>
- ⁵⁰ C. A. Lipinski, F. Lombardo, B. W. Dominy and P. J. Feeney, *Adv. Drug Deliv. Rev.*, **46**, 3 (2001), [https://doi.org/10.1016/s0169-409x\(00\)00129-0](https://doi.org/10.1016/s0169-409x(00)00129-0)